Materials Today: Proceedings xxx (xxxx) xxx

Contents lists available at ScienceDirect

Materials Today: Proceedings

journal homepage: www.elsevier.com/locate/matpr

Investigation on microstructure and hardness of nickel-alumina functionally graded material

S.N.S. Jamaludin [a,*], M.I.A. Latiff [b], D.M. Nuruzzaman [b], N.M. Ismail [b], S. Basri [c]

[a] Faculty of Engineering, DRB-HICOM University of Automotive Malaysia, 26607 Pekan, Pahang, Malaysia
[b] Faculty of Manufacturing Engineering, University Malaysia Pahang, 26600 Pekan, Pahang, Malaysia
[c] Faculty of BioEngineering and Technology, University Malaysia Kelantan, Kelantan, Malaysia

ARTICLE INFO

Article history:
Available online xxxx

Keywords:
Microstructure
Hardness
Nickel-alumina
Functionally graded material
Powder Metallurgy

ABSTRACT

In this research study, six-layered nickel-alumina (Ni-Al_2O_3) functionally graded material (FGM) was prepared using powder metallurgy (PM) method. The objectives of this study were to investigate the microstructure and hardness of the graded composite layer by layer. Using a cylindrical steel die, the six-layered nickel-alumina graded structure was fabricated considering 0%, 20%, 40%, 60%, 80% and 100% weight percentage of ceramic concentration for different layers. A hydraulic press was used for fabrication of the FGM layered structure and 30 ton compaction load was applied. Considering two-step sintering cycle, sintering was carried out at sintering temperature 1200 °C and sintering time 4 h. The sintered specimens were characterized using optical microscopy (OM), scanning electron microscopy (SEM) and hardness testing. It was observed that uniform particle distribution within the graded layers and smooth microstructural transition occurred between adjacent layers. It was also observed that the interface lines are obvious, less wavy, straight and parallel which confirms proper layer stacking process. On the other hand, from the SEM micrographs, the existence of microcracks and voids are identified in the alumina-rich layer and mostly around alumina particles.

Selection and peer-review under responsibility of 4th Advanced Materials Conference 2018, 4th AMC 2018, 27th & 28th November 2018, Hilton Kuching Hotel, Kuching, Sarawak, Malaysia.

1. Introduction

In recent years, there is an increasing need for development of new materials for different types of engineering applications. A homogeneous material of uniform structure cannot fulfill the requirements simultaneously. Functionally graded material (FGM) which possesses multifunctional properties can satisfy the requirements under extreme environments and this material combines the good properties of both ceramic and metal. Within FGM, the inhomogeneous composition gradually varies from one side to another along the thickness direction. This graded structure can be continuous or stepwise which improves the bonding between constituent elements and reduces the stress at the interface. In order to process these graded composite materials, various methods were followed such as thermal spraying, centrifugal casting, vapor deposition and powder metallurgy [1–5]. In order to produce the inhomogeneous graded composite system, nowadays powder metallurgy method is widely used to fulfill the required characteristics by controlling the properties of each constituent element. Sintering process is one of the challenging steps in order to prepare the multi-layered graded composite structure free of defects. Cracks and camber are prevalent due to the residual stress caused by the mismatches in thermal expansion and sintering between successive layers [6–8].

The properties of multi-layered functional materials of different combinations were investigated experimentally and theoretically [9–14]. Mechanical responses of these composite systems significantly influenced by layer number, sintering condition, compaction load, material composition, sintering atmosphere etc. Mechanical properties of aluminium based graded composite systems were investigated [15]. The obtained results revealed that the hardness of outer parts of composites is higher than that of middle or inner parts. It was also reported that the strength of the outer region is higher than that of inner region. Recently, using centrifugal casting method, Al/SiC graded composite material was prepared and the properties such as, microstructure, hardness and wear were investigated [16]. It was reported that the properties of the graded

* Corresponding author.
E-mail address: sakinah@dhu.edu.my (S.N.S. Jamaludin).

https://doi.org/10.1016/j.matpr.2020.05.644
2214-7853/
Selection and peer-review under responsibility of 4th Advanced Materials Conference 2018, 4th AMC 2018, 27th & 28th November 2018, Hilton Kuching Hotel, Kuching, Sarawak, Malaysia.

composites were influenced by particle volume fraction, applied load, sliding speed etc. By applying laser melting deposition method, stainless steel graded parts were fabricated and the microstructures were analyzed [17]. It was reported that strong bonding was achieved between substrate and deposited material. Recently, six-layered nickel-alumina graded composite structure was prepared using pressureless sintering under argon atmosphere [18]. The obtained results revealed that smooth transition occurred from one layer to next layer and microstructural observation confirmed the successful of compaction process. Aluminum/high-density polyethylene graded composite panel was analyzed both theoretically and experimentally [19]. From the analyses it was confirmed that theoretical predictions are matched with the experimental results.

Despite the previous investigations, characteristics of six-layered nickel-alumina functionally graded composite structure were not clearly understood. Therefore, in this research study, six-layered nickel-alumina graded composite structure was prepared using powder metallurgy method under two-step pressureless sintering. Physical properties, microstructural characteristics and hardness were analysed layer by layer. Interfacial characteristics were also examined in this study.

2. Experimental

Functionally graded nickel-alumina (Ni-Al_2O_3) samples had been fabricated via conventional powder processing route followed by pressureless sintering technique. Six layered samples were constructed which consisted of pure Ni layer on one end and pure Al_2O_3 layer on the other, linked by 4 graded layers having the composition of Ni uniformly changing by 20 wt%. The constituent powders used are high purity nickel and alumina (Sigma Aldrich, USA). The average particle size of Ni is 40–50 μm and Al_2O_3 is 60–70 μm. The constituent powders were first weighed according to the respective molecular weight percentage (wt.%) assigned for each individual layer. Then the weighed powders were mixed thoroughly following the proportion of the layer mixtures and crushed using mortar and pestle until homogeneous and no agglomerate is visible. The powder mixtures were then sieved through a 100 μm mesh sieve and subsequently dried in an oven at 100 °C for 1 h to remove moisture. The powder mixtures were stacked layer by layer in a cylindrical die of radius 15 mm in order to produce the green compact. Al_2O_3 layer was placed first on the bottom while Ni layer on top near the upper punch. This is due to higher rigidity of Al_2O_3 compared to Ni, so the Ni layer will retain in shape and did not collapse after compaction. Fig. 1 shows the schematic arrangement of the apparatus as well as the Ni/Al_2O_3 green body configuration in the die.

After all the layers had been stacked inside the die, the green body was subjected to uniaxial compaction at pressure of 30 ton (414 MPa) using a hydraulic press (TOYO: Model TL30, capacity: 30 tonne). The pressure was increased gradually to reach 30 tonne in order to avoid failures in the FGM structure and the structure was allowed to settle at 30 tonne before it was taken out. Then the mass and dimensions of green compacts were measured. The green compact produced was relatively fragile and had low cohesive strength. To increase the samples strength, the green compacts were sintered to 1200 °C for 4 h in a tube furnace (Elite Thermal Systems Limited). The sintering process was done in argon controlled atmosphere by flowing argon gas at the rate of 50–55 ml/min before starting and throughout the heating cycle. The heating up and cooling down rate were set at 4 °C/min and 2 °C/min, respectively. The sintering curve also included a preheating stage at 150 °C for 30 min for the removal of moisture and

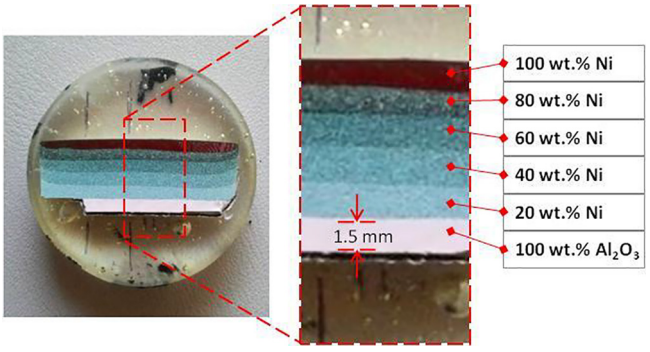

Fig. 2. Cross sectional view of 6 layered Ni-Al_2O_3 FGM sample and the layers specification.

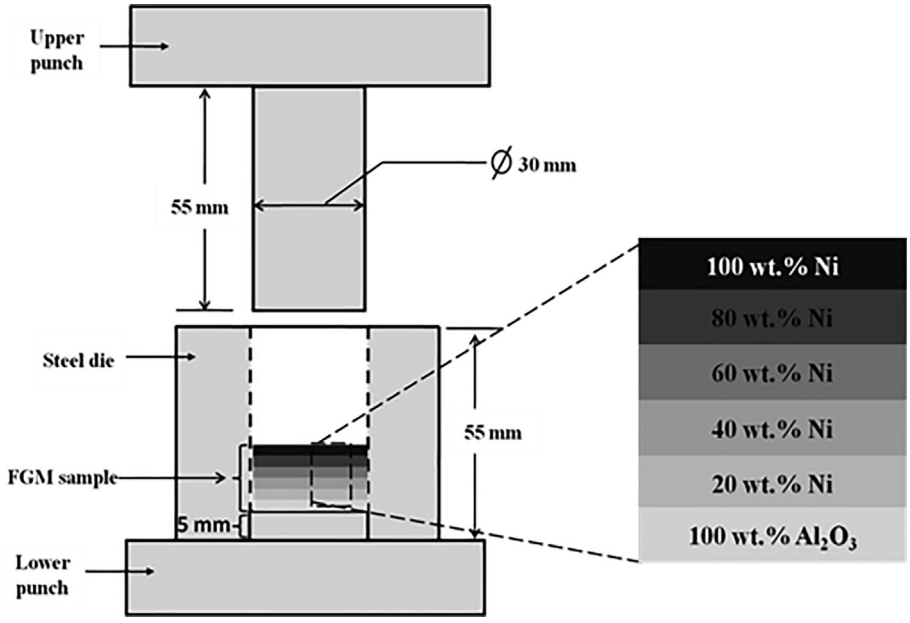

Fig. 1. Schematic arrangement of the 15 mm radius cylindrical die and the configuration of functionally graded Ni-Al_2O_3 sample.

Please cite this article as: S. N. S. Jamaludin, M. I. A. Latiff, D. M. Nuruzzaman et al., Investigation on microstructure and hardness of nickel-alumina functionally graded material, Materials Today: Proceedings, https://doi.org/10.1016/j.matpr.2020.05.644

chemical impurities from the sample. After fabrication, the sintered samples were consecutively cut on the cross-sectional direction, mounted in polymer resin, ground with emery paper and finally polished to 0.3 μm using polishing powder. Fig. 2 shows the cross-sectional view of the sintered 6 layered Ni-Al_2O_3 FGM sample mounted inside polymer resin. The individual layers can easily be identified due the difference in the colors of each layer hence the percentage compositions for individual layers are labelled. The average thickness of each layer measured using optical microscope is 1.5 mm, building up the samples of average total thickness around 9.0 mm.

The prepared samples were characterized for physical and microstructural characteristics. Samples density, porosity and shrinkage were determined for the physical characterization [20,21]. The diameters of FGM samples before and after sintering at the top (0 wt% Al_2O_3), mid (60 wt% Al_2O_3) and bottom positions (100 wt% Al_2O_3) were measured and the changes in the dimensions calculated to determine the shrinkage percentage. The dimensions of diameters were chosen because for cylindrical specimens, length on the diametric direction is usually the greatest and would therefore provide the most accurate measurement for shrinkage. Shrinkage percentages for both sintering conditions can be expressed as a percentage of sintered length from the following equation:

$$Shrinkage(\%) = \frac{l_s - l_g}{l_g} \times 100$$

where ℓ_g is the initial green compact length, ℓ_s is the sintered length and ℓ_s - ℓ_g is the change in length due to heat treatment process.

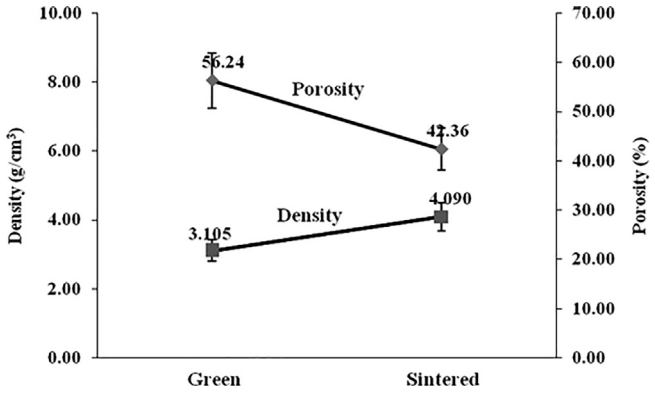

Fig. 3. Changes in density and porosity between green compacts and sintered samples of 6 layered Ni-Al2O3 FGM.

Optical micrograph images were obtained using Olympus microscope (model BX51M) while Scanning Electron Microscopic (SEM) images were acquired using SEM) machine (model FEI Quanta 450). The hardness for every layer of FGM samples was measured using Wilson Vicker's micro-hardness testing machine (maximum test load 2 kgf). The hardness measurement was performed at an applied load of 1kgf (9.8 N) for dwell time 15 s [10]. The average of at least three values was taken as the result to ensure accuracy.

3. Results and discussion

Fig. 3 shows the changes in density and porosity between green compacts and sintered samples of Ni-Al_2O_3 FGM. The sintered density increased to 4.090 g/cm^3 from the density of green compact which is 3.105 g/cm^3. Accordingly, the porosity of sintered samples decreased 13.88% compared to the green compacts. Although decreased, the amounts of porosities in the sintered bodies were still high might be because the composite phases could not be consolidated to full density [18,22].

The solidification mechanism experienced during sintering stage caused the samples to shrink due to the elimination of pores and formation of Ni and Al_2O_3 particles bonding [23]. Fig. 4 shows the slanted shape along the side planes of whereby the diameter at the top side (Ni) is larger than the diameter at the bottom side (Al_2O_3).

Fig. 5 shows the diameter variations at three different positions between green and sintered samples. It can be seen that the

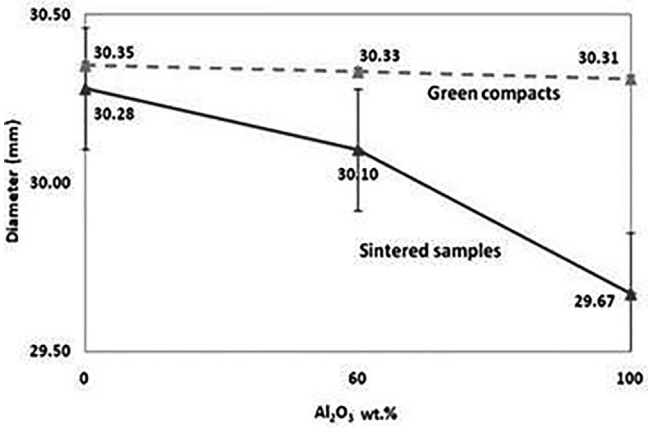

Fig. 5. Diameter variation between green compact and sintered samples of 6 layered Ni-Al_2O_3 FGM.

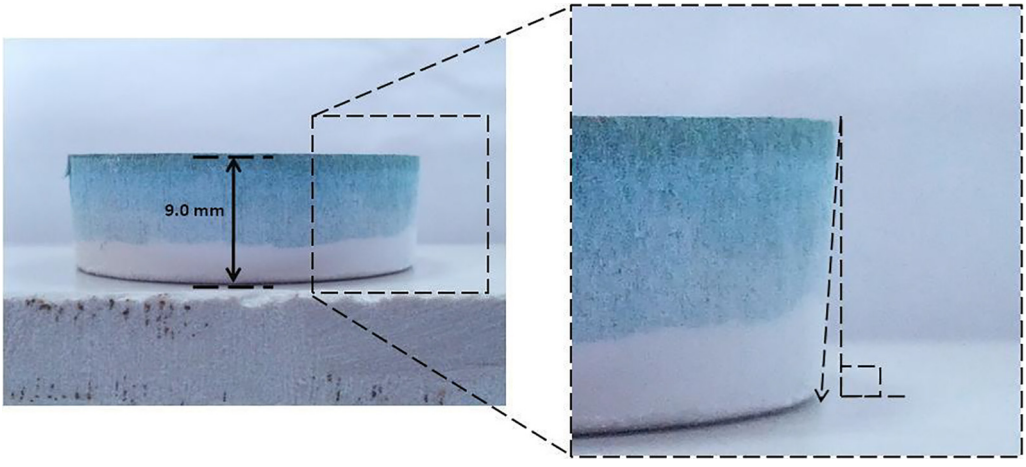

Fig. 4. Shrinkage of Ni-Al_2O_3 FGM sintered samples viewed from the front and magnified image showing the slanted side plane.

Please cite this article as: S. N. S. Jamaludin, M. I. A. Latiff, D. M. Nuruzzaman et al., Investigation on microstructure and hardness of nickel-alumina functionally graded material, Materials Today: Proceedings, https://doi.org/10.1016/j.matpr.2020.05.644

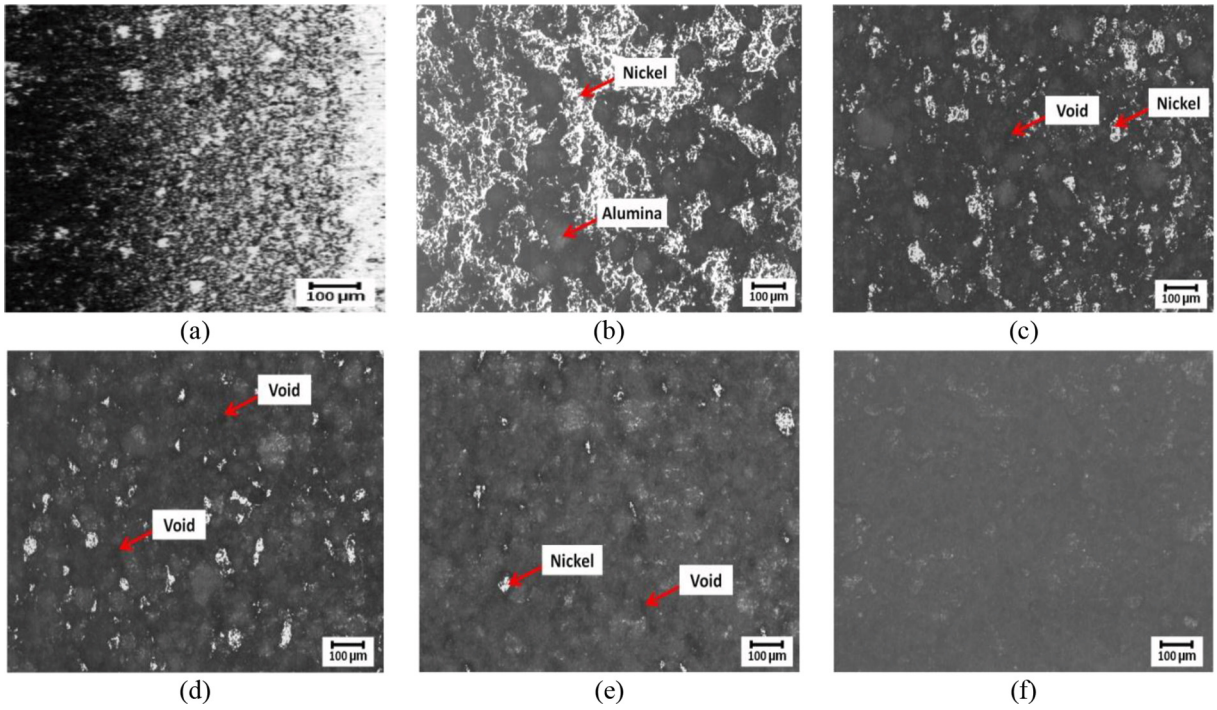

Fig. 6. Optical micrographs for every layer in the 6 layered Ni-Al_2O_3 FGM (a)100 wt% Ni (b) 80 wt% Ni (c) 60 wt% Ni (d) 40 wt% Ni (e) 20 wt% Ni (f) 100 wt% Al_2O_3.

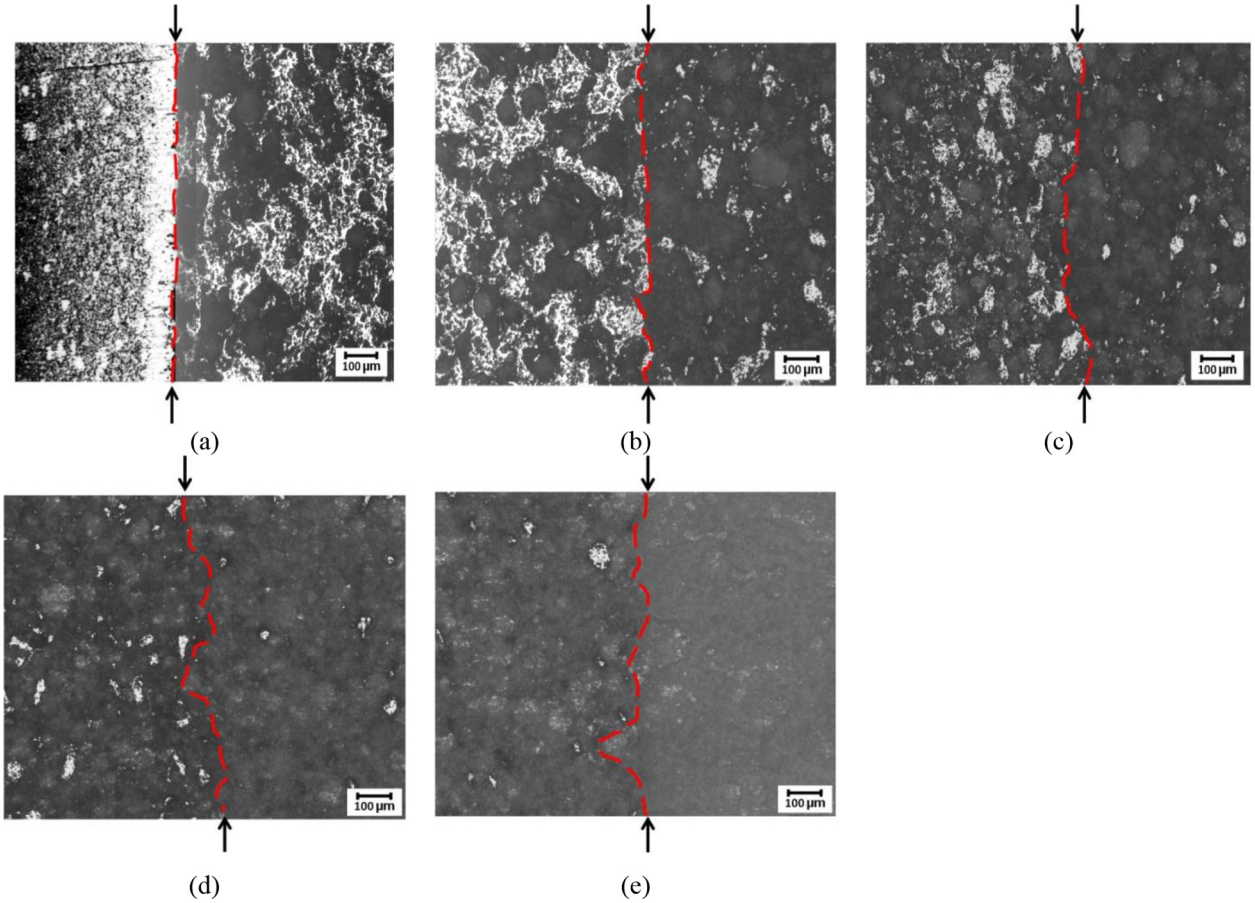

Fig. 7. Optical micrographs near the interfaces in the 6 layered Ni-Al_2O_3 FGM (a) 100 wt% Ni + 80 wt% Ni (b) 80 wt% Ni + 60 wt% Ni (c) 60 wt% Ni + 40 wt% Ni (d) 40 wt% Ni + 20 wt% Ni (e) 20 wt% Ni + 100 wt% Al_2O_3.

Please cite this article as: S. N. S. Jamaludin, M. I. A. Latiff, D. M. Nuruzzaman et al., Investigation on microstructure and hardness of nickel-alumina functionally graded material, Materials Today: Proceedings, https://doi.org/10.1016/j.matpr.2020.05.644

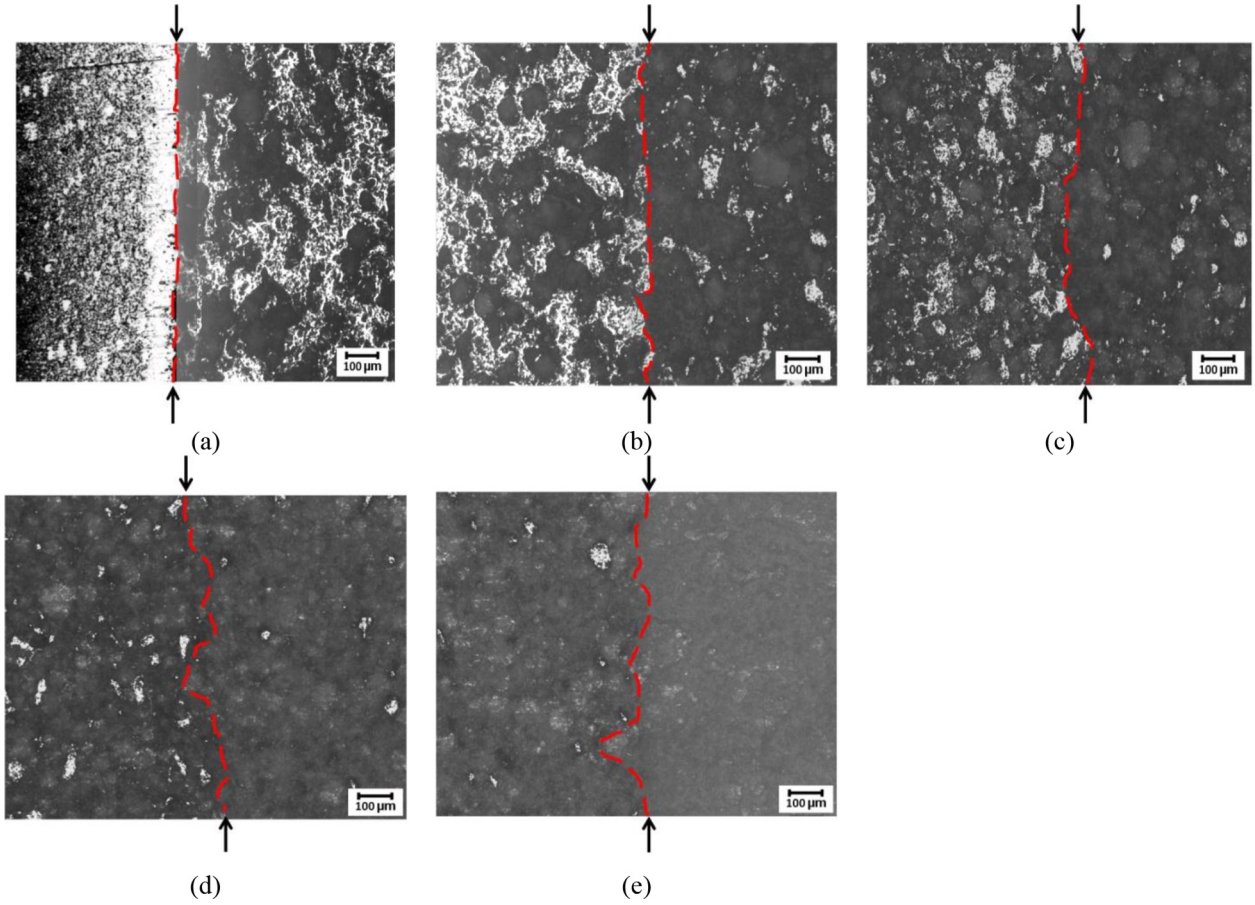

Fig. 8. SEM images of 6 layered Ni-Al_2O_3 FGM samples near the interfaces (a)100 wt% Ni + 80 wt% Ni (b) 60 wt% Ni + 40 wt% Ni (c) 20 wt% Ni + 100 wt% Al_2O_3.

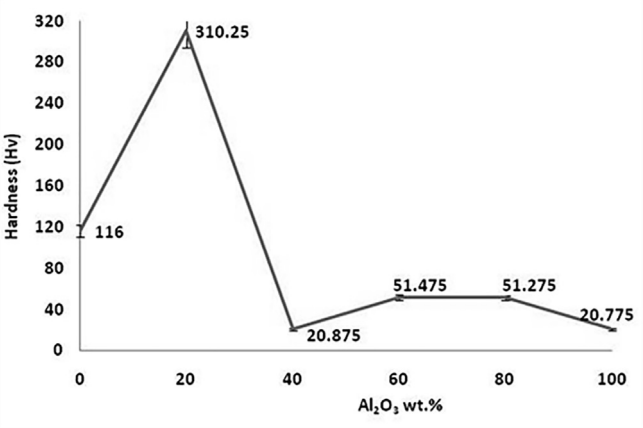

Fig. 9. Microhardness variation trends at each discrete layer in Ni-Al_2O_3 samples.

diameter of the sample is decreasing as the composition of Al_2O_3 was increasing which implies that more porosities in the layers were eliminated during solidification process [24]. This phenomenon occurred due to the large difference in the sintering behaviour between nickel and alumina compositions whereby the porosities in the nickel-rich layers do not consumed as much as those in the alumina-rich layers. However it is important to point that for the alumina-rich layers, low sintering temperature used in the fabrication process might also be the reason to limit the sintering behaviour in the alumina-rich compositions [21].

The following Fig. 6(a)-(f) show the optical micrograph image of individual layer for the 6-layered FG sample. In the following micrographs, the shiny and bright particles are identified as metal (Ni) phases while darker regions represent the ceramic (Al_2O_3) phases. However, due to the increased ceramic composition and decreased Ni particles, Al_2O_3 phases become more visible due to the lighting adjustment. At 80 wt% Ni composition, larger volume of metal represents the matrix phase while ceramic presents as the reinforcing phase. Thus various sizes of ceramic particles and agglomerates can be seen dispersed in the interconnected Ni phases. The metal networks gradually disconnected and isolated as the composition of alumina was increased even at 60 wt% Ni layer because of high volume of ceramic powders in the layer mixtures. Consequently, Ni particles are viewed as the reinforcement phases while dispersed Al_2O_3 particles begin to combine and form clusters. The microstructural characteristic of Al_2O_3 changed from a dispersed type structure to an aggregated structure. In 40 wt% Ni layer, Al_2O_3 clusters formed into long-range interconnected structures known as percolated cluster structures. Accordingly, Ni phases interconnectivity broke into aggregated structures, then into discrete Ni grains in the 20 wt% Ni layer. These microstructural characteristics of the graded structure are in agreement with the microstructural characterization of eight layered nickel-alumina FGM by previous investigation [21].

Fig. 7(a)-(e) show the interfacial lines in the 6 layered Ni-Al_2O_3 FGM sample. The interfacial barriers and gradually varied layer compositions separating the pure metal and ceramic layers confirmed the construction of FGM. At the interfaces, smooth transition of microstructures can be observed between one layer to the next and this gradually varied microstructure can be observed more clearly in the SEM images (Fig. 8). This confirms the proper stacking process of powder materials also. The constructed dashed lines which represent the interface boundaries are mostly straight

Please cite this article as: S. N. S. Jamaludin, M. I. A. Latiff, D. M. Nuruzzaman et al., Investigation on microstructure and hardness of nickel-alumina functionally graded material, Materials Today: Proceedings, https://doi.org/10.1016/j.matpr.2020.05.644

and parallel to each other, judging from the positions of the arrows on both sides of each micrograph which have close parallel gaps. The waviness of interfacial boundaries is considered normal occurrences in powder stacking process that indicates non-uniformity in the layer thickness as powders were stacked before compaction.

Ni-Al_2O_3 FGM samples were also examined using SEM analysis to observe the cross sectional surfaces at the higher resolution and magnification. Beside the surface topography, SEM images also capable to identify different phases of compositions by assigning different colour in the images. Fig. 8 shows different layers in Ni-Al_2O_3 FGM samples under SEM. Ni phases are assigned as bright and white regions while Al_2O_3 phases are assigned as dark and grey. Smooth microstructural transitions i.e gradual change in microstructure between adjacent layers as observed from the optical images (Fig. 7) are clearer in the SEM micrographs. The interface lines are almost parallel with each other and less wavy as compared to those in the optical images. This confirms a good interfacial solid state bonding between Ni and Al_2O_3 constituents and proper layer stacking process. At 80 wt% Ni layer (a), there are long connection of Al_2O_3 particles can be observed which formed the aggregated Al_2O_3 structures. In the 60 wt% Ni layer, Ni and Al_2O_3 exist as big and separate particles. The big Al_2O_3 particles then predominate and formed matrix phase with the inclusions of separated Ni particles. In the adjacent layer with 20 wt% Ni, the Ni particles dispersed throughout the Al_2O_3 matrix. In the SEM micrographs, microcracks and voids in the composite layers can be observed more clearly. Voids or pores were left in the sintered body due to the particle diffusions between metal-ceramic constituents at the final stage of sintering process [25]. Microcracks which mostly observed around Al_2O_3 particles were formed due to incomplete transformation of ceramic phases into hard ceramic [18].

Fig. 9 illustrates the microhardness variation trends at each discrete layer in Ni-Al_2O_3 samples sintered for 4 h sintering time. The microhardness values increased significantly from 116.00 Hv at the pure Ni layer to 310.25 Hv of 20 wt% Al_2O_3 layer. This indicates that the increase in alumina content will increase the hardness value, provided that the layer mixture is fully sintered. However this value decreased drastically to 20.875 Hv when moving to the adjacent layer, a sign of porous structure and incomplete densification [18,24]. As the ceramic contents increased, the apparent viscosity of matrix increased which also enhanced the chances of air entrapment in the structure post sintering [12]. The lowest hardness value was also observed at pure Al_2O_3 layer (20.78 Hv). The incomplete densification of Al_2O_3 phases can also be related to the presence of microcracks particularly around the Al_2O_3 particles as observed from SEM micrographs.

4. Conclusion

Physical and microstructural properties of 6 layered Ni/Al_2O_3 functionally graded samples produced by powder metallurgy and pressureless sintering processes had been studied. From the micrographs, the pattern of microstructural changes across all layers from fully metal to fully ceramic can be observed. In terms of the ceramic composition changes, the optical images showed that the ceramic reinforcement phases initially existed as dispersed particles then gradually building the aggregated network type structure until ceramic phases became the dominant matrix with dispersed Ni particles. The interfacial boundaries were generally straight and parallel to each other and also showed smooth microstructural transition between adjacent layers. The SEM micrographs revealed the presence of microcracks and voids particularly in the alumina-rich layer and mostly around alumina particles. Besides the fact that the ceramic phases were not able to be sintered into hard ceramic, it is believed that these microcracks and voids affected the low results in sample microhardness.

Acknowledgements

This research work was performed under the IRGS/012017/009 grant and the authors are grateful to DRB-HICOM University of Automotive Malaysia for the financial support. The authors also acknowledge the assistance by the technical staffs of the faculty of manufacturing engineering, University Malaysia Pahang (UMP).

References

[1] Y. Watanabe, Y. Hattori, H. Sato, J. Mater. Process. Technol. 221 (2015) 197–204.
[2] K. Wu, S. Scheler, H.S. Park, M.W. Porada, J. Eur. Ceram. Soc. 33 (2013) 1111–1121.
[3] M.S. EL-Wazery, A.R. EL-Desouky, O.A. Hamed, A. Fathy, N.A. Mansour, Int. J. Eng. Trans. A: Basics 26 (2013) 375–382.
[4] W.M. Rubio, G.H. Paulino, E.C.N. Silva, Mater. Des. 41 (2012) 255–256.
[5] A.M. Khoddami, A. Sabour, S.M.M. Hadavi, Surf. Coat. Technol. 201 (2007) 6019–6024.
[6] A. Shahrjerdi, F. Mustapha, M. Bayat, S.M. Sapuan, D.L.A. Majid, Int. J. Phys. Sci. 6 (2011) 2258–2267.
[7] L. Sun, A. Sneller, P. Kwon, Mater. Sci. Eng., A 488 (2008) 31–38.
[8] M.I.A. Latiff, S.N.S. Jamaludin, S. Basri, A. Hussain, D.S. Al-Othmany, F. Mustapha, D.M. Nuruzzaman, N.M. Ismail, I. Ismail, Appl. Mech. Mater. 629 (2014) 437–443.
[9] L. Tahvilian, Z.Z. Fang, Mater. Sci. Eng., A 557 (2012) 106–112.
[10] F. Erdemir, A. Canakci, T. Varol, Trans. Nonferrous Met. Soc. China 25 (2015) 3569–3577.
[11] S.N.S. Jamaludin, S. Basri, A. Hussain, D.S. Al-Othmany, F. Mustapha, D.M. Nuruzzaman, Math. Probl. Eng. 2014 (2014) 1–20.
[12] M. Bhattacharyya, A.N. Kumar, S. Kapuria, Mater. Sci. Eng. A 487 (2008) 524–535.
[13] S.S. Hosseini, H. Bayesteh, S. Mohammadi, Mater. Sci. Eng. A 561 (2013) 285–302.
[14] S.N.S. Jamaludin, S. Basri, F. Mustapha, D.M. Nuruzzaman, M.I.A. Latiff, N.M. Ismail, Mater. Sci. Forum. 889 (2017) 90–95.
[15] N. Radhika, R. Raghu, Trans. Nonferr. Met. Soc. China 26 (2016) 905–916.
[16] T.R. Prabhu, Arch. Civ. Mech. Eng. 17 (2017) 20–31.
[17] C.H. Zhang, H. Zhang, C.L. Wu, S. Zhang, Z.L. Sun, S.Y. Dong, Vacuum 141 (2017) 181–187.
[18] M.I.A. Latiff, D.M. Nuruzzaman, S. Basri, N.M. Ismail, S.N.S. Jamaludin, F.F. Kamaruzaman, IOP Conf. Ser. Mater. Sci. Eng. 342 (2018) 1–8.
[19] Q. Lin, F. Chen, H. Yin, Eng. Struct. 138 (2017) 17–26.
[20] J.C. Lee, S.H. Ahn, Int. J. Precis. Eng. Man. 19 (2018) 31–37.
[21] M.L. Pines, H.A. Bruck, Acta Mater. 54 (2006) 1457–1465.
[22] S.Y. Gomez, D. Hotza, J. Eur. Ceram. Soc. 38 (2018) 1736–1741.
[23] V.G. Karayannis, A.K. Moutsatsou, Adv. Mater. Sci. Eng. 2012 (2012) 1–9.
[24] Y.V. Bykov, S.V. Egorov, A.G. Eremeev, V.V. Holoptsev, I.V. Plotnikov, K.I. Rybakov, V.E. Semenov, A.A. Sorokin, J. Mater. Process. Technol. 214 (2014) 210–216.
[25] A. Yusefi, N. Parvin, Fusion Eng. Des. 114 (2017) 196–202.

Please cite this article as: S. N. S. Jamaludin, M. I. A. Latiff, D. M. Nuruzzaman et al., Investigation on microstructure and hardness of nickel-alumina functionally graded material, Materials Today: Proceedings, https://doi.org/10.1016/j.matpr.2020.05.644